Journal Name

ARTICLE TYPE

Cite this: DOI: 10.1039/xxxxxxxxxx

Modeling Excitation Energy Transfer in Multi-BODIPYs Architectures: Electronic Supplementary Information (ESI)

Cloé Azarias,[a] Roberto Russo,[b] Lorenzo Cupellini,[b] Benedetta Mennucci,*[b] and Denis Jacquemin*[ac]

[a] *Chimie Et Interdisciplinarité, Synthèse, Analyse, Modélisation (CEISAM), UMR CNRS no. 6230, BP 92208, Université de Nantes, 2, Rue de la Houssinière, 44322 Nantes, France. E-mail: Denis.Jacquemin@univ-nantes.fr*

[b] *Dipartimento di Chimica e Chimica Industriale, University of Pisa, Via Moruzzi 3, 56124 Pisa, Italy. E-mail: Benedetta.Mennucci@unipi.it*

[c] *Institut Universitaire de France, 1 rue Descartes, F-75231 Paris Cedex 05, France.*

S1 Spectral overlap in 1a-H$^+$

One observes in Table S1 that computing the spectral overlap either from the spectra of the protonated species (**1a-H**$^+$) or from the shifted spectra of the non-protonated species (**1a**) leads to similar spectral overlaps and consequently, similar EET rate constants. This outcome enables to validate the strategy proposed in Section 2.2 in the main text to compute the spectral overlap of the newly proposed species.

Table S1 Theoretical EET rate constants ($k^{th.}$ in s^{-1}) between the first excited-states of the donor and acceptor moieties for the protonated **1a-H**$^+$ and non-protonated **1a** dyad. The spectral overlap has been either taken directly from the experimental spectra of the protonated species (J in cm^{-1}) or from the shifted spectra of the non-protonated species ($J_{shifted}$ in cm^{-1}). The shifts (ΔE^X in eV) have been computed according to the TD-DFT transition energies ($E^X_{S_1}$ in eV) of the donor (X=D) and acceptor (X=A) moieties

Molecule	$E^D_{S_1}$	$E^A_{S_1}$	ΔE^D	ΔE^A	J	$J_{shifted}$	$k^{th.}$ in s^{-1}
1a	2.86	2.35	—	—	7.8×10^{-5}	—	8.0×10^{9}
1a-H$^+$	2.86	2.55	—	—	2.3×10^{-4}	—	2.4×10^{10}
	2.86	2.55	0.00	0.20	—	2.4×10^{-4}	2.5×10^{10}

S2 Nomenclature of the fragments

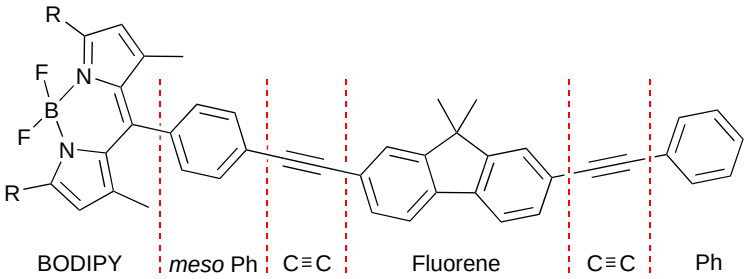

Fig. S1 Representation of the different fragments considered for **1a**.

S3 Different models used to compute EET in 1a

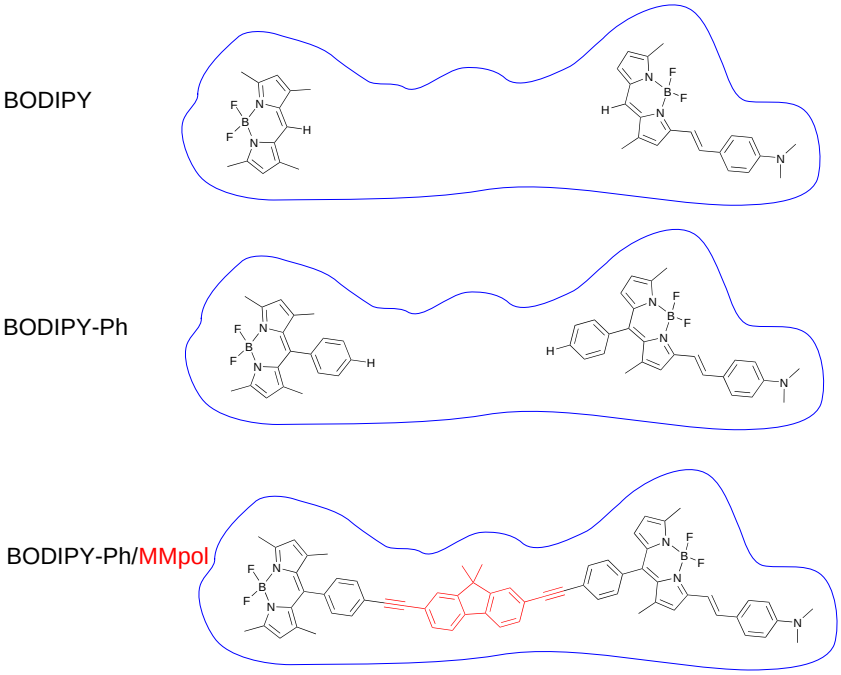

Fig. S2 Representation of the different models employed to compute EET coupling in **1a**. The blue line represents the PCM cavity surrounding the molecule. The black color indicates that the fragment is computed at a QM level whereas the red color indicates that the fragment is modeled with the MMpol scheme.

S4 Rotational analysis in 1a

In Table S2, we report the couplings (V^{Coul}, V^{PCM} and V^{Tot}) and the EET rate constants of the different rotamers of **1a**.

Table S2 Theoretical couplings (V in cm^{-1}) and EET rate constants ($k^{\mathrm{th.}}$ in s^{-1}) between the first excited-states of the donor and acceptor moieties for different rotamers considered in the **1a** dyad (see Figure 3 in the main text)

Increments on Φ_A (°)	0	30	60	90	120	150	180	210	240	270	300	330
V^{Coul}	14.0	11.7	6.2	1.1	8.2	13.3	14.9	12.6	7.1	0.2	7.4	12.4
V^{PCM}	-4.7	-3.9	-2.0	-0.4	-2.8	-4.5	-5.1	-4.3	-2.4	-0.0	-2.5	-4.2
V^{Tot}	9.3	7.8	4.2	0.7	5.4	8.7	9.8	8.3	4.7	0.2	4.9	8.2
$k^{\mathrm{th.}}$	8.0×10^9	5.6×10^9	1.6×10^9	4.2×10^7	2.7×10^9	7.0×10^9	8.9×10^9	6.4×10^9	2.0×10^9	2.0×10^6	2.2×10^9	6.3×10^9
Increments on Φ_D (°)	0	30	60	90	120	150	180	210	240	270	300	330
V^{Coul}	14.0	13.7	9.7	3.1	4.4	10.7	14.3	14.0	10.0	3.4	4.1	10.7
V^{PCM}	-4.7	-4.7	-3.4	-1.3	-1.3	-3.5	-4.8	-4.8	-3.6	-1.4	-1.2	-3.4
V^{Tot}	9.3	9.0	6.3	1.8	3.1	7.2	9.4	9.2	6.4	2.0	3.0	7.1
$k^{\mathrm{th.}}$	8.0×10^9	7.5×10^9	3.7×10^9	3.0×10^8	9.1×10^8	4.8×10^9	8.2×10^9	7.7×10^9	3.8×10^9	3.7×10^8	8.1×10^8	4.6×10^9

S5 Effect of the counter-ion in 1a-H$^+$

In Figure S3, the different optimized conformations of the counter-ion (triflic acid, $SO_3CF_3^-$) are presented. For all of them, we computed the exact same values of the couplings (14.9, 4.9 and 10.0 cm^{-1}, for V^{Coul}, V^{PCM} and V^{Tot}, respectively) and consequently the same value of the EET rate constant, 2.6 x 10^{10} s^{-1}. This value is very similar to the one obtained with **1a-H**$^+$ (2.3 x 10^{10} s^{-1}), *i.e.*, when the $SO_3CF_3^-$ ion is not explicitly included in the model. Therefore the counter-ion has a trifling impact on both the electronic and energy transfer properties.

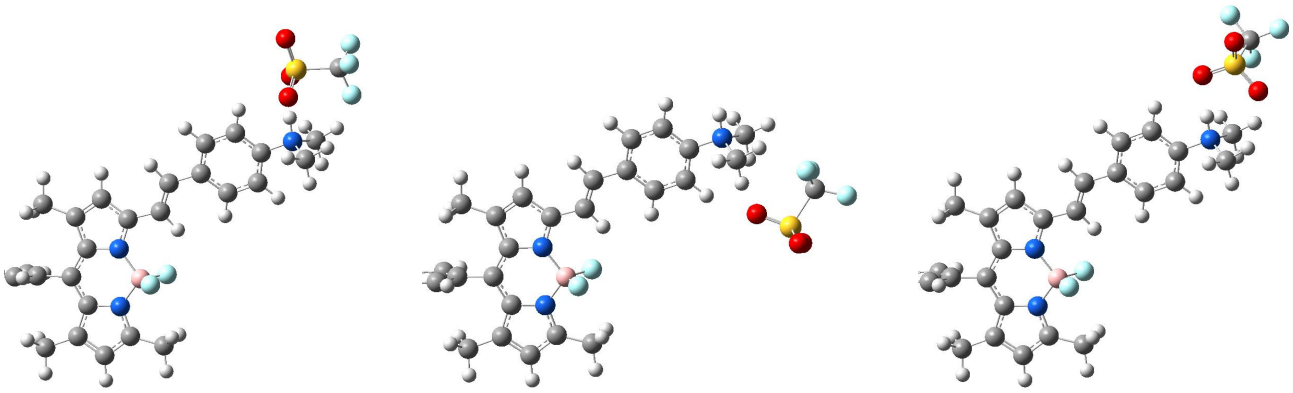

Fig. S3 Representation of the different optimized conformation of the counter-ion in **1a-H**$^+$.

S6 Orientation of the bipy terminal groups in 1b

We optimized the **1b** dyad with different conformations of the bipy groups (see Figure S4). In Figure S5, we display the NTO orbital pairs associated to the first singlet excitation of the acceptor fragment in **1b** and in **1b-l**. One sees that the topology of the orbital localized on the terminal nitrogen atom slightly differs between the two conformers. The biggest change appears in the "particle" case where the orbital on the nitrogen atom is slight deformed in **1b** compared to **1b-l**. We also computed the Merz-Kollman charges for the atoms in these two fragments. It turns out that the charge on the terminal nitrogen atom varies from 0.11 e in **1b** to 0.39 e in **1b-l**.

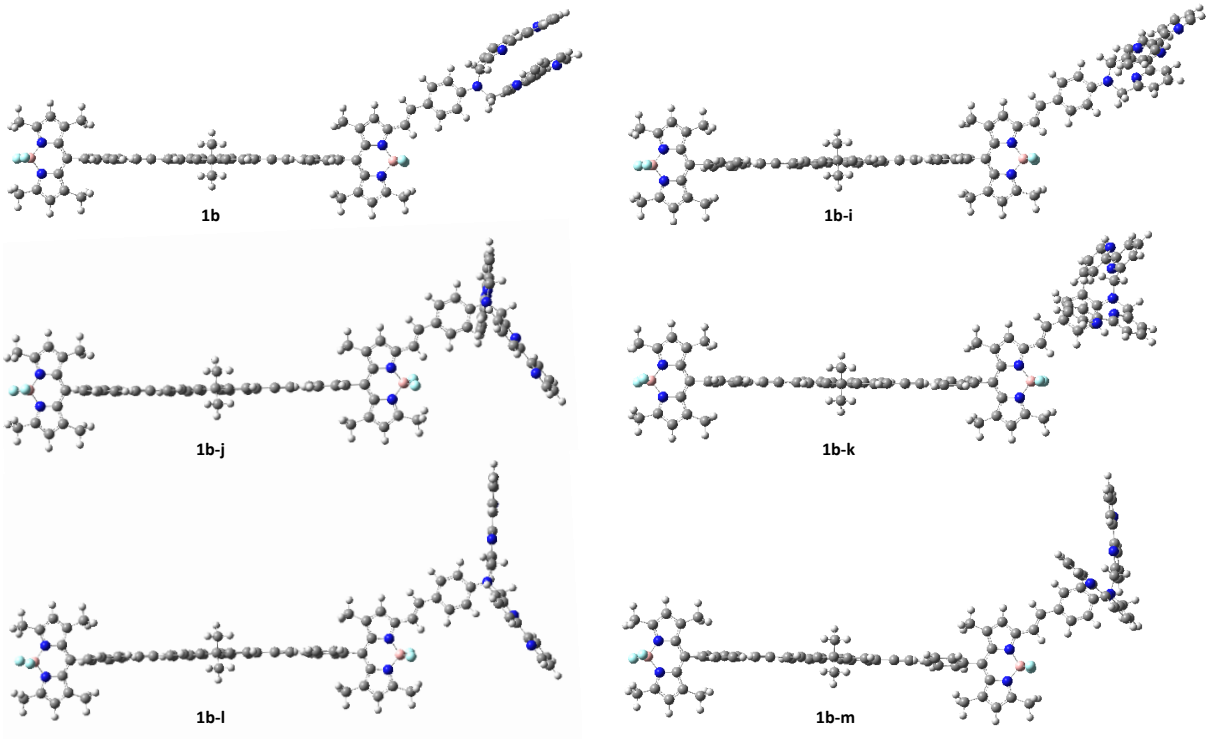

Fig. S4 Representation of the optimized conformers for **1b**.

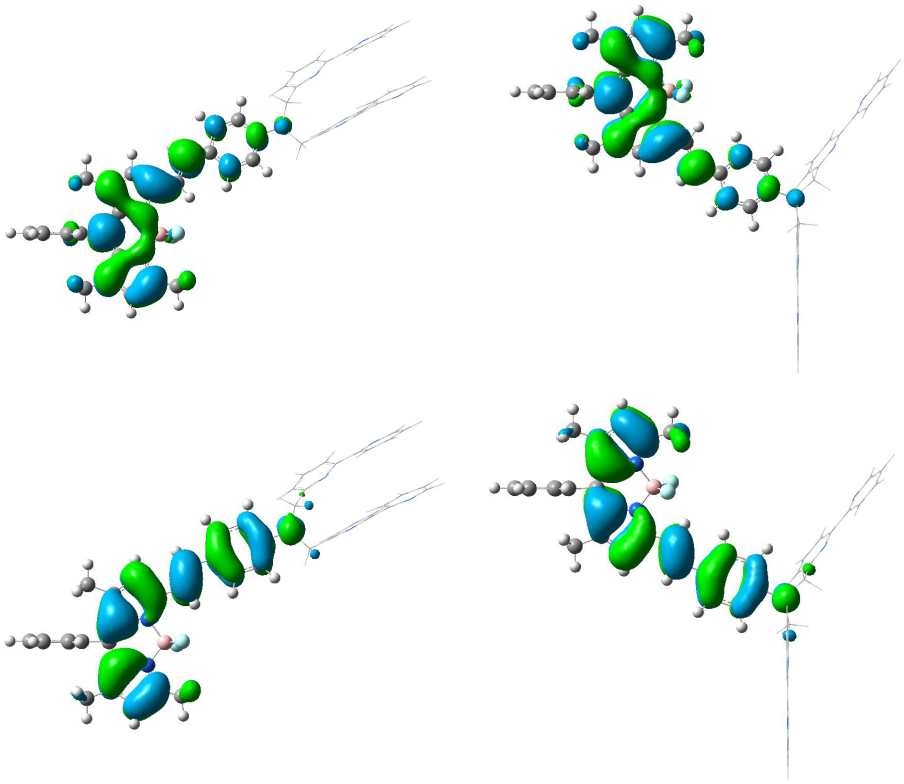

Fig. S5 The dominant natural transition orbital pairs (isovalue=0.02 a.u.) for the first singlet excited-states of **1b** (left) and **1b-l** (right). For each state, the "hole" is at the top, the "particle" at the bottom. The associated eigenvalues are 0.98. For the sake of clarity, we have represented the groups attached to the terminal nitrogen usign the so-called wireframe description.

S7 Rotational analysis in 3

In Table S3, we report the couplings (V^{Coul}, V^{PCM} and V^{Tot}) and the EET rate constants of the different rotamers of the fragments **I** and **J** in **3**. Note that the structure used in this analysis has been simplified: the bipy groups were replaced by hydrogen atoms for the sake of saving computational time.

Table S3 Theoretical couplings (V in cm^{-1}) and EET rate constants ($k^{th.}$ in s^{-1}) between the first excited-states of the donor **I** and acceptor **J** moieties for different rotamers considered in the **3** triad

Increments on Φ_J (°)	0	30	60	90	120	150	180	210	240	270	300	330
V^{Coul}	7.8	13.0	12.7	7.1	2.4	13.8	23.7	29.3	28.5	22.2	12.5	1.7
V^{PCM}	-1.1	-3.5	-3.5	-1.2	-2.9	-7.9	-12.4	-14.9	-14.7	-12.0	-7.9	-3.2
V^{Tot}	6.7	9.5	9.2	6.0	0.5	5.9	11.4	14.4	13.8	10.1	4.6	1.5
$k^{th.}$	1.7×10^{10}	3.4×10^{10}	3.2×10^{10}	1.3×10^{10}	9.4×10^{7}	1.3×10^{10}	4.8×10^{10}	7.7×10^{10}	7.2×10^{10}	3.9×10^{10}	7.9×10^{9}	8.1×10^{8}

S8 Optimized structures of 3, 4 and 5

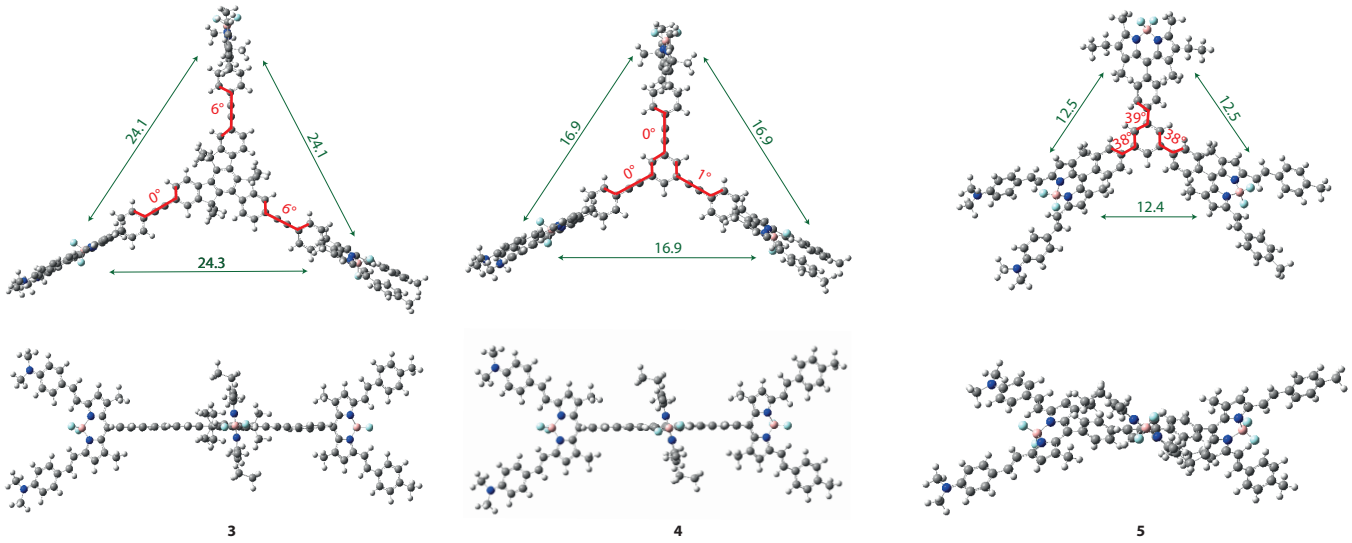

Fig. S6 Side (top) and top (bottom) view of the optimized structure of **3**, **4** and **5**. The distances (in Å) between the *meso* carbon atoms of the BODIPYs are given in green whereas the dihedral angles between the bridge and the *meso* phenyl of the BODIPYs are given in red.

S9 Additional data for structures designed from 3

In Table S4, we report the transition energies of each fragment in the designed triads derived from **3**. It turns out that, for **3-H**$_2^{2+}$, **3b**, **3b-H**$^+$ and **3c-H**$^+$, the proposed chemical change leads to an inversion in the transition energy between fragments **L** and **M**, and consequently, to an inversion of the energy transfer direction between these two BODIPYs. Table S4 also lists the relative electronic energies between the two key conformers of **3c** represented in Figure S7 and its protonated counterpart **3c-H**$^+$. The difference between the two conformers (in both non-protonated and protonated forms) is negligible and both forms co-exist in solution. The EET rate constant reported for **3c** and **3c-H**$^+$ in the main text is consequently determined as the mean value of the rates obtained for the two conformers.

Table S4 Relative electronic energy ($E_{rel.}$ in kcal.mol^{-1}) and electronic transition energy ($E^{\mathbf{X}}_{S_1}$ in eV) of each fragment **X** in the designed triad derived from **3**. The **3c** key conformers are represented in Figure S7 The values in bold correspond to an inversion in the energy transition between two fragments

Molecule	$E_{rel.}$	$E^{\mathbf{K}}_{S_1}$	$E^{\mathbf{L}}_{S_1}$	$E^{\mathbf{M}}_{S_1}$
3	—	2.74	2.22	2.03
3-H$^+$	—	2.73	2.21	2.10
3-H$_2^{2+}$	—	2.73	**2.21**	**2.26**
3a	—	2.74	2.49	2.03
3a-H$^+$	—	2.74	2.49	2.10
3a-H$_2^{2+}$	—	2.73	2.49	2.25
3b	—	2.74	**2.21**	**2.34**
3b-H$^+$	—	2.74	**2.21**	**2.52**
3c$_1$	0.03	2.74	2.49	2.34
3c$_2$	0.00	2.74	2.49	2.34
3c$_1$**-H**$^+$	0.00	2.74	**2.49**	**2.52**
3c$_2$**-H**$^+$	0.02	2.74	**2.49**	**2.54**

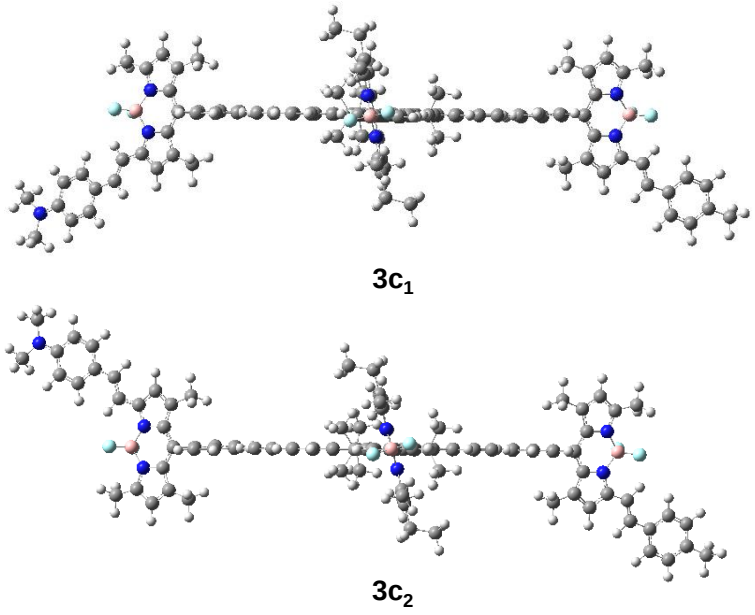

Fig. S7 Representation of the optimized conformers of the **3c** structure.

Table S5 Theoretical couplings (V in cm^{-1}), spectral overlap (J in cm) and EET rate constants ($k^{th.}$ in s^{-1}) in the new structures derived from **3** (see Figure 6 in the body of the text). The directionality of the energy transfer from the donor part (D) to the acceptor part (A), denoted D→A, is reported according to the computed transition energies (see Table S4). The rotational conformers of **3c**, namely **3c**$_1$ and **3c**$_2$, are displayed in Figure S7

Molecule	D→A	V^{Coul}	V^{PCM}	V^{Tot}	J	$k^{th.}$
3	**K→L**	17.3	-7.2	10.1	1.2×10^{-4}	1.4×10^{10}
	K→M	17.0	-7.2	9.9	3.2×10^{-5}	3.7×10^{9}
	L→M	18.7	-7.9	10.8	2.6×10^{-4}	3.6×10^{10}
3-H$^+$	**K→L**	16.1	-6.7	9.4	1.2×10^{-4}	1.3×10^{10}
	K→M	14.9	-6.2	8.7	5.5×10^{-5}	5.0×10^{9}
	L→M	18.8	-8.0	10.8	3.2×10^{-4}	4.3×10^{10}
3-H$_2^{2+}$	**K→L**	16.0	-6.6	9.4	1.2×10^{-4}	1.2×10^{10}
	K→M	16.7	-6.9	9.8	1.5×10^{-4}	1.7×10^{10}
	M→L	19.0	-7.9	11.1	1.8×10^{-4}	2.7×10^{10}
3a	**K→L'**	14.7	-5.9	8.8	3.6×10^{-4}	3.3×10^{10}
	K→M	16.3	-6.9	9.5	3.2×10^{-5}	3.4×10^{9}
	L'→M	17.7	-7.4	10.3	4.4×10^{-5}	5.5×10^{9}
3a-H$^+$	**K→L'**	14.6	-5.9	8.7	3.6×10^{-4}	3.3×10^{10}
	K→M	17.1	-7.3	9.8	5.5×10^{-5}	6.3×10^{9}
	L'→M	21.0	-9.4	11.5	7.4×10^{-5}	1.2×10^{10}
3a-H$_2^{2+}$	**K→L'**	14.3	-5.7	8.6	3.6×10^{-4}	3.1×10^{10}
	K→M	14.9	-6.1	8.8	1.4×10^{-4}	1.3×10^{10}
	L'→M	17.6	-7.2	10.4	2.1×10^{-4}	2.7×10^{10}
3b	**K→L**	16.7	-6.9	9.8	1.2×10^{-4}	1.3×10^{10}
	K→M'	16.3	-6.8	9.5	2.2×10^{-4}	2.3×10^{10}
	M'→L	17.0	-7.1	9.9	4.1×10^{-4}	4.7×10^{10}
3b-H$^+$	**K→L**	16.6	-6.9	9.7	1.2×10^{-4}	1.3×10^{10}
	K→M'	16.0	-6.5	9.4	3.2×10^{-4}	3.4×10^{10}
	M'→L	17.2	-7.0	10.1	2.1×10^{-4}	2.5×10^{10}
3c$_1$	**K→L'**	14.9	-6.0	8.9	3.6×10^{-4}	3.4×10^{10}
	K→M'	16.4	-6.9	9.5	2.2×10^{-4}	2.3×10^{10}
	L'→M'	26.0	-12.4	13.7	2.8×10^{-4}	6.2×10^{10}
3c$_2$	**K→L'**	13.9	-5.6	8.4	3.6×10^{-4}	3.0×10^{10}
	K→M'	12.7	-5.1	7.6	2.2×10^{-4}	1.5×10^{10}
	L'→M'	6.8	-1.0	5.8	2.8×10^{-4}	1.1×10^{10}
3c$_1$-H$^+$	**K→L'**	14.1	-5.6	8.5	3.6×10^{-4}	3.1×10^{10}
	K→M'	15.2	-6.2	9.0	3.2×10^{-4}	3.1×10^{10}
	M'→L'	21.1	-9.6	11.5	1.3×10^{-4}	2.1×10^{10}
3c$_2$-H$^+$	**K→L'**	13.9	-5.5	8.3	3.6×10^{-4}	3.0×10^{10}
	K→M'	12.1	-4.7	7.4	3.2×10^{-4}	2.0×10^{10}
	M'→L'	9.9	-2.8	7.1	1.7×10^{-4}	1.0×10^{10}

S10 Additional data for non-protonated and protonated structures designed from 4

In Table S6, we report the transition energies of each fragment in the designed triads derived from **4** as well as the relative electronic energies between the **4c** conformers depicted in Figure S8. Alike the compounds derived from **3**, the inversion in the energy transfer direction between **L** and **M** is observed for the same chemical changes, *i.e.* for molecules **4-H**$_2^{2+}$, **4b**, **4b-H**$^+$ and **4c-H**$^+$, and the EET rate constant for **4c** and **4c-H**$^+$ reported in the body of the text corresponds to the mean value of the rates obtained for their two conformers.

Table S6 Relative electronic energy ($E_{rel.}$ in kcal.mol^{-1}) and electronic transition energy ($E^{X}_{S_1}$ in eV) of each fragment **X** in the designed triad derived from **4**. The **4c** key conformers are represented in Figure S8 The values in bold correspond to an inversion in the transition energy of the two fragments

Molecule	$E_{rel.}$	$E^{K}_{S_1}$	$E^{L}_{S_1}$	$E^{M}_{S_1}$
4	—	2.74	2.22	2.03
4-H$^+$	—	2.73	2.22	2.10
4-H$_2^{2+}$	—	2.74	**2.21**	**2.26**
4a	—	2.74	2.50	2.03
4a-H$^+$	—	2.73	2.49	2.10
4a-H$_2^{2+}$	—	2.74	2.49	2.25
4b	—	2.74	**2.22**	**2.34**
4b-H$^+$	—	2.74	**2.22**	**2.53**
4c$_1$	0.01	2.74	2.50	2.34
4c$_2$	0.00	2.73	2.49	2.34
4c$_1$**-H**$^+$	0.00	2.74	**2.49**	**2.52**
4c$_2$**-H**$^+$	0.01	2.73	**2.49**	**2.52**

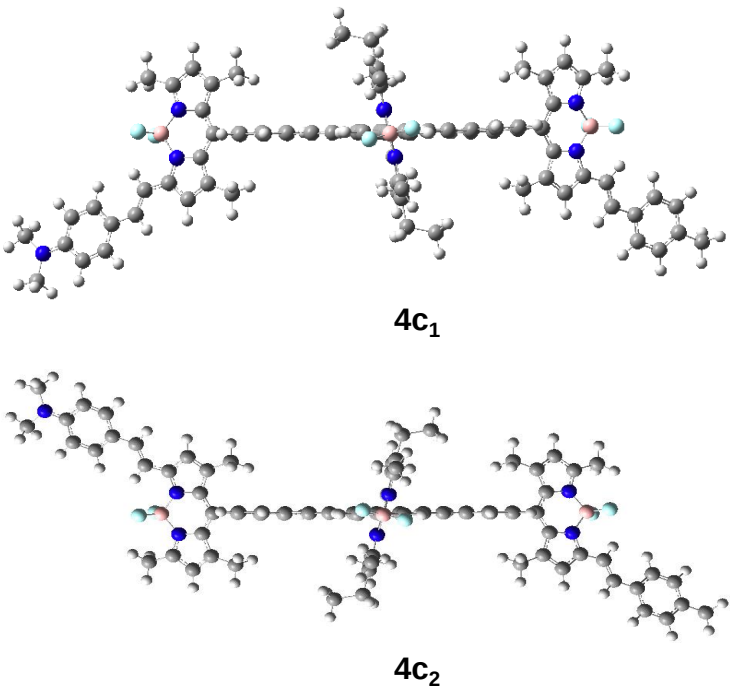

Fig. S8 Representation of the optimized conformers of the **4c** structure.

Table S7 Theoretical couplings (V in cm^{-1}), spectral overlap (J in cm) and EET rate constants ($k^{th.}$ in s^{-1}) in the new structures derived from **4** (see Figure 6 in the body of the text). The directionality of the energy transfer from the donor part (D) to the acceptor part (A), denoted D→A, is reported according to the computed transition energies (see Table S6). The rotational conformers of **4c**, namely **4c**$_1$ and **4c**$_2$, are displayed in Figure S8

Molecule	D→A	V^{Coul}	V^{PCM}	V^{Tot}	J	$k^{th.}$
4	**K→L**	37.7	-15.7	22.1	1.2×10^{-4}	6.9×10^{10}
	K→M	36.6	-15.4	21.2	3.3×10^{-5}	1.7×10^{10}
	L→M	39.9	-16.9	23.1	2.6×10^{-4}	1.6×10^{11}
4-H$^+$	**K→L**	37.2	-15.4	21.8	1.2×10^{-4}	6.7×10^{10}
	K→M	30.7	-12.8	17.9	5.5×10^{-5}	2.1×10^{10}
	L→M	34.1	-14.4	19.7	3.1×10^{-4}	1.4×10^{11}
4-H$_2^{2+}$	**K→L**	35.6	-14.7	20.9	1.2×10^{-4}	6.1×10^{10}
	K→M	25.1	-10.1	14.9	1.4×10^{-4}	3.8×10^{10}
	M→L	25.1	-10.3	14.8	1.7×10^{-4}	4.4×10^{10}
4a	**K→L'**	39.3	-16.2	23.0	3.6×10^{-4}	2.3×10^{11}
	K→M	37.8	-15.9	21.9	3.2×10^{-5}	1.8×10^{10}
	L'→M	37.7	-15.5	22.2	4.3×10^{-5}	2.5×10^{10}
4a-H$^+$	**K→L'**	36.7	-15.0	21.7	3.6×10^{-4}	2.0×10^{11}
	K→M	29.6	-12.3	17.3	5.5×10^{-5}	1.9×10^{10}
	L'→M	17.0	-5.4	11.6	7.3×10^{-5}	1.1×10^{10}
4a-H$_2^{2+}$	**K→L'**	37.9	-15.6	22.3	3.6×10^{-4}	2.1×10^{11}
	K→M	39.7	-16.6	23.1	1.4×10^{-4}	8.5×10^{10}
	L'→M	39.1	-16.0	23.1	2.1×10^{-4}	1.3×10^{11}
4b	**K→L**	38.3	-15.9	22.4	1.2×10^{-4}	7.0×10^{10}
	K→M'	37.0	-15.4	21.6	2.2×10^{-4}	1.2×10^{11}
	M'→L	35.5	-14.7	20.9	4.0×10^{-4}	2.1×10^{11}
4b-H$^+$	**K→L**	37.8	-15.7	22.1	1.2×10^{-4}	6.9×10^{10}
	K→M'	33.9	-13.7	20.1	3.2×10^{-4}	1.5×10^{11}
	M'→L	33.5	-13.5	20.0	2.0×10^{-4}	9.4×10^{10}
4c$_1$	**K→L'**	35.1	-14.2	20.9	3.6×10^{-4}	1.9×10^{11}
	K→M'	36.8	-15.3	21.4	2.2×10^{-4}	1.2×10^{11}
	L'→M'	58.7	-27.3	31.4	2.8×10^{-4}	3.3×10^{11}
4c$_2$	**K→L'**	38.0	-15.6	22.4	3.6×10^{-4}	2.1×10^{11}
	K→M'	37.5	-15.8	21.7	2.2×10^{-4}	1.2×10^{11}
	L'→M'	9.3	-0.2	9.1	2.8×10^{-4}	2.8×10^{10}
4c$_1$**-H**$^+$	**K→L'**	34.5	-14.0	20.6	3.6×10^{-4}	1.8×10^{11}
	K→M'	37.7	-15.5	22.2	3.2×10^{-4}	1.9×10^{11}
	M'→L'	51.1	-22.9	28.2	1.4×10^{-4}	1.3×10^{11}
4c$_2$**-H**$^+$	**K→L'**	37.1	-15.2	21.9	3.6×10^{-4}	2.1×10^{11}
	K→M'	38.4	-15.9	22.5	3.2×10^{-4}	1.9×10^{11}
	M'→L'	19.3	-5.3	14.0	1.4×10^{-4}	3.3×10^{10}

S11 Additional EET data for non-protonated and protonated structures designed from 5

In Table S8, we report the transition energies of each fragment in the designed triads derived from **5** and the relative energies between the key conformers displayed in Figures S9, S10, S11, S12 and S13. Alike the compounds derived from **3** and **4**, the inversion in the energy transfer direction between **L** and **M** is observed for the same chemical changes, *i.e.* for molecules **5-H**$_2^{2+}$, **5b**, **5b-H**$^+$ and **5c-H**$^+$, and the EET rate constant for **5-H**+, **5a**, **5a-H**$^+$, **5a-H**$_2^{2+}$ **5b**, **5b-H**+, **5c** and **5c-H**+ reported in the body of the text corresponds to the mean value of the rates obtained for their conformers.

Table S8 Relative electronic energy ($E_{rel.}$ in kcal.mol^{-1}) and electronic transition energy ($E^{\mathbf{X}}_{S_1}$ in eV) of each fragment **X** in the designed triad derived from **5**. See below for the representation of the different conformers. The values in bold correspond to an inversion in the transition energy of two fragments

Molecule	$E_{rel.}$	$E^{\mathbf{K}}_{S_1}$	$E^{\mathbf{L}}_{S_1}$	$E^{\mathbf{M}}_{S_1}$
5	—	2.73	2.22	2.03
5-H$_a^+$	0.00	2.73	2.22	2.10
5-H$_b^+$	0.00	2.73	2.21	2.10
5-H$_2^{2+}$	—	2.73	**2.21**	**2.26**
5a$_1$	0.01	2.73	2.49	2.03
5a$_2$	0.00	2.73	2.49	2.03
5a$_1$**-H**$_a^+$	0.03	2.74	2.49	2.10
5a$_1$**-H**$_b^+$	0.02	2.73	2.49	2.10
5a$_2$**-H**$_a^+$	0.00	2.74	2.49	2.10
5a$_2$**-H**$_b^+$	0.00	2.74	2.49	2.10
5a$_1$**-H**$_2^{2+}$	0.13	2.74	2.49	2.25
5a$_2$**-H**$_2^{2+}$	0.00	2.74	2.49	2.25
5b$_1$	0.03	2.73	**2.22**	**2.34**
5b$_2$	0.00	2.74	**2.21**	**2.34**
5b$_1$**-H**$^+$	0.00	2.74	**2.22**	**2.52**
5b$_2$**-H**$^+$	0.06	2.74	**2.21**	**2.53**
5c$_1$	0.03	2.73	2.49	2.34
5c$_2$	0.04	2.73	2.49	2.34
5c$_3$	0.00	2.73	2.50	2.34
5c$_4$	0.01	2.74	2.50	2.34
5c$_1$**-H**$^+$	0.05	2.74	**2.49**	**2.53**
5c$_2$**-H**$^+$	0.01	2.74	**2.49**	**2.52**
5c$_3$**-H**$^+$	0.02	2.73	**2.49**	**2.52**
5c$_4$**-H**$^+$	0.00	2.73	**2.49**	**2.53**

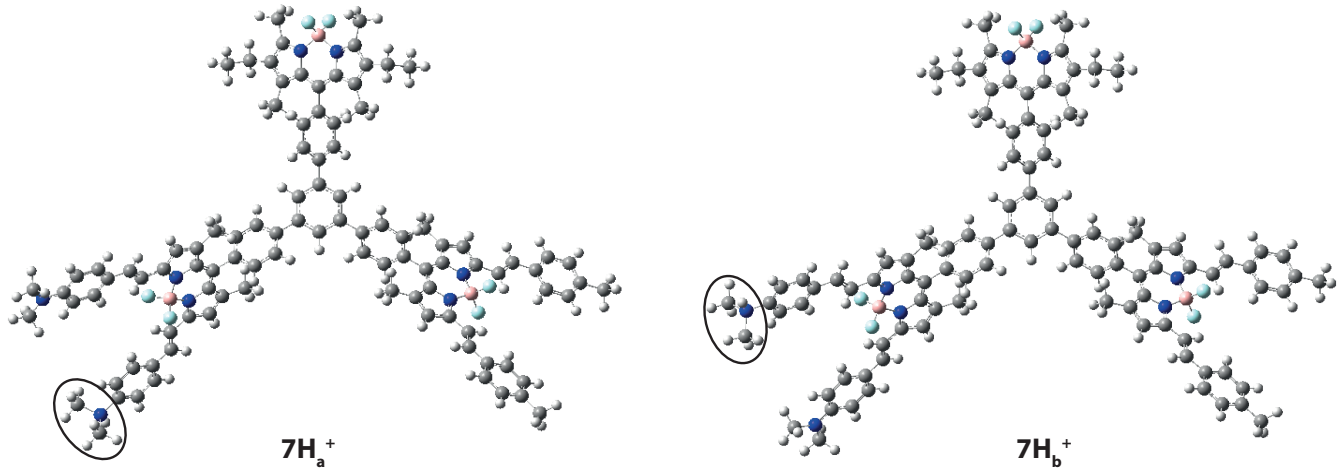

Fig. S9 Representation of the optimized conformers of the **5-H**$^+$ structures. The protonated amino group has been circled.

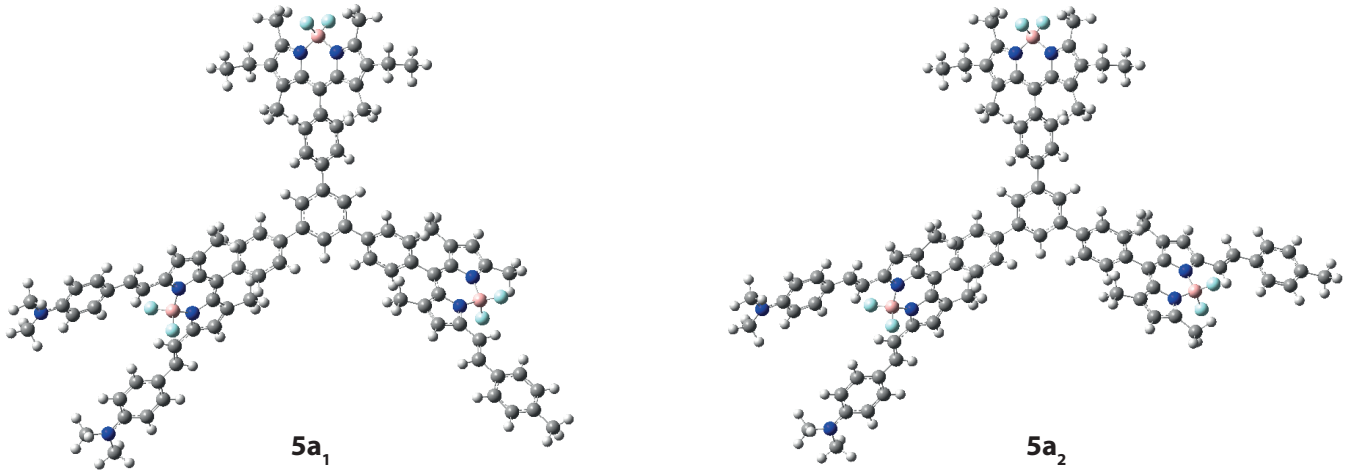

Fig. S10 Representation of the two optimized conformers of **5a**.

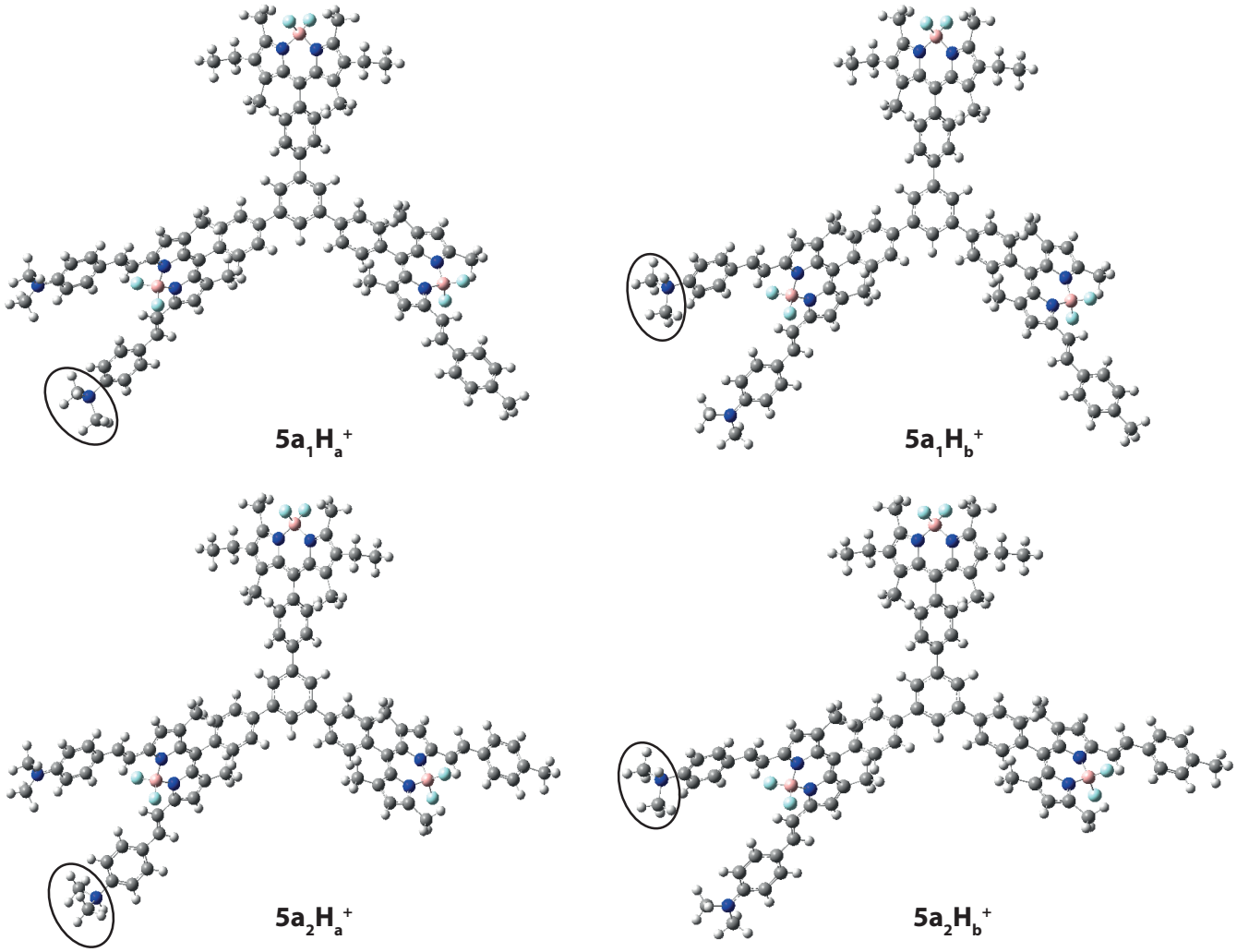

Fig. S11 Representation of the optimized conformers of **5a-H**$^{+}$. The protonated amino group has been circled.

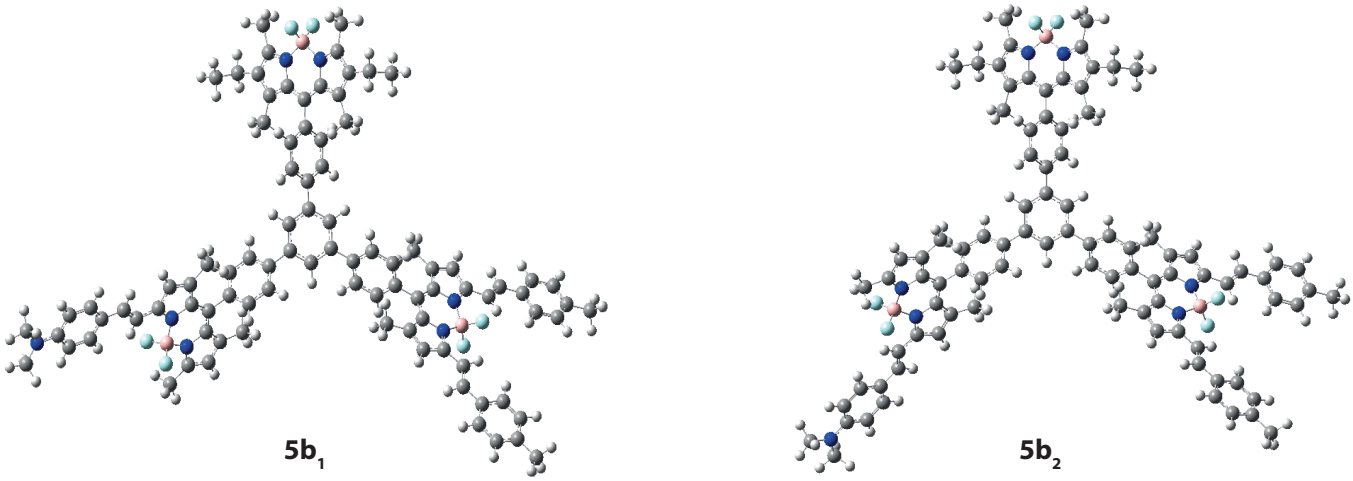

Fig. S12 Representation of the two optimized conformers of **5b**.

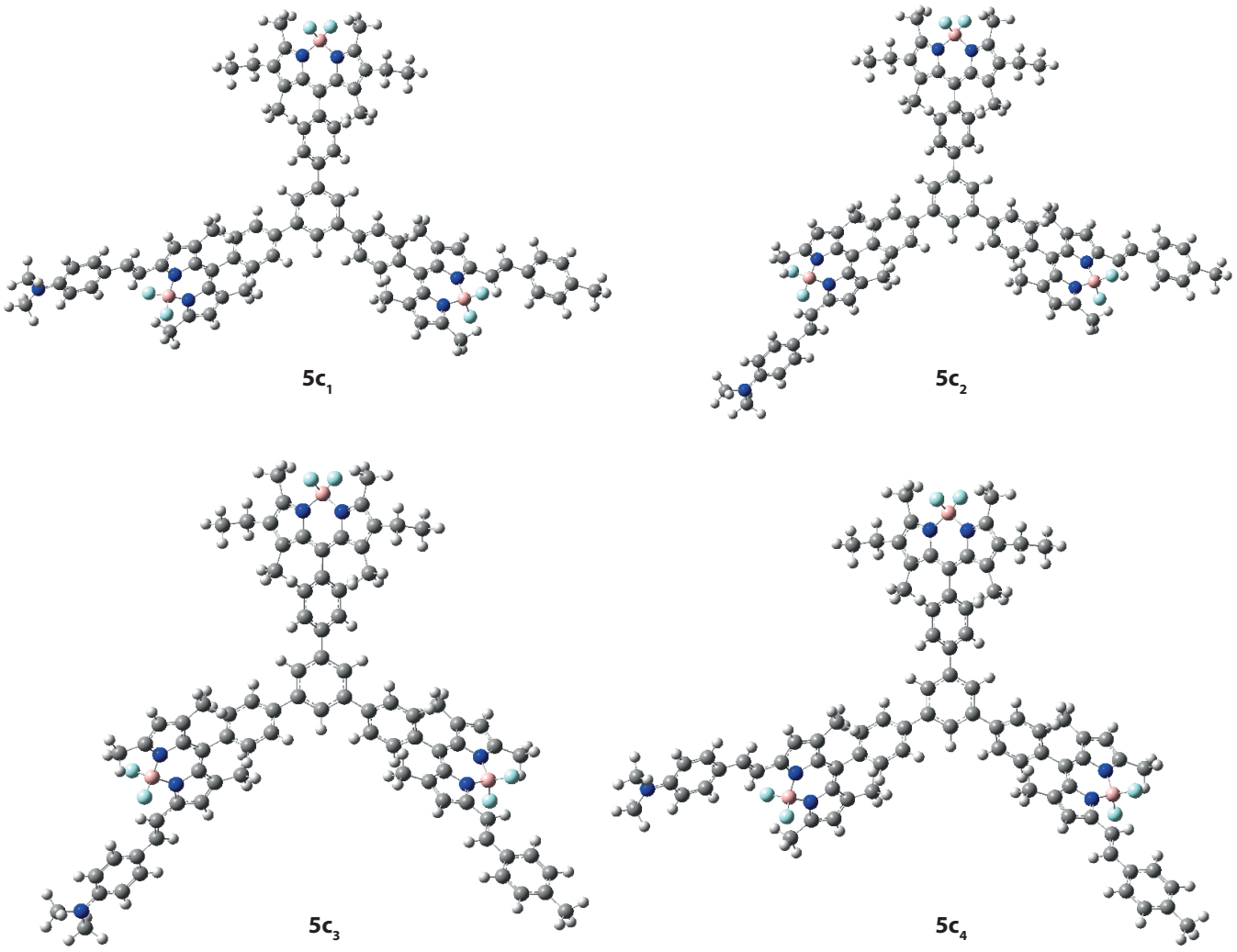

Fig. S13 Representation of the optimized conformers of **5c**.

Table S9 Theoretical couplings (V in cm^{-1}), spectral overlap (J in cm) and EET rate constants ($k^{th.}$ in s^{-1}) in the structures derived from **5** (see Figure 6 in the body of the text). The directionality of the energy transfer from the donor part (D) to the acceptor part (A), denoted D→A, is reported according to the computed transition energies (see Table S8). The rotational conformers are displayed in Figures S9-S13

Molecule	D→A	V^{Coul}	V^{PCM}	V^{Tot}	J	$k^{th.}$
5	**K→L**	14.3	-7.7	6.6	1.2×10^{-4}	6.1×10^{9}
	K→M	13.8	-7.3	6.4	3.3×10^{-5}	1.6×10^{9}
	L→M	1.2	-1.1	0.1	2.6×10^{-4}	1.4×10^{6}
5-H$_a^+$	**K→L**	13.0	-7.2	5.9	1.2×10^{-4}	4.9×10^{9}
	K→M	1.7	-2.1	-0.5	5.5×10^{-5}	1.4×10^{7}
	L'→M	4.7	-2.4	2.3	3.1×10^{-4}	2.0×10^{9}
5-H$_b^+$	**K→L**	17.3	-9.0	8.3	1.2×10^{-4}	9.7×10^{9}
	K→M	22.7	-11.0	11.7	5.6×10^{-5}	8.9×10^{9}
	L'→M	4.0	-0.8	3.2	3.1×10^{-4}	3.7×10^{9}
5-H$_2^{2+}$	**K→L**	7.5	-2.0	5.6	1.2×10^{-4}	4.4×10^{9}
	K→M	14.5	-7.5	6.6	1.4×10^{-4}	7.5×10^{9}
	M→L	19.9	-7.7	12.1	1.8×10^{-4}	3.1×10^{10}
5a$_1$	**K→L'**	32.4	-15.3	17.1	3.6×10^{-4}	1.2×10^{11}
	K→M	12.9	-6.8	6.1	3.3×10^{-5}	1.5×10^{9}
	L'→M	1.6	0.4	2.0	4.5×10^{-5}	2.1×10^{8}
5a$_2$	**K→L'**	0.3	-1.5	-1.2	3.6×10^{-4}	6.1×10^{8}
	K→M	14.2	-7.6	6.6	3.3×10^{-5}	1.7×10^{9}
	L'→M	14.5	-6.6	7.9	4.4×10^{-5}	3.3×10^{9}
5a$_1$-H$_a^+$	**K→L'**	31.1	-14.8	16.3	3.6×10^{-4}	1.1×10^{11}
	K→M	0.6	1.0	1.6	5.5×10^{-5}	1.7×10^{8}
	L'→M	17.5	-8.9	8.6	7.3×10^{-5}	6.4×10^{9}
5a$_1$-H$_b^+$	**K→L'**	32.7	-15.4	17.2	3.6×10^{-4}	1.3×10^{11}
	K→M	26.9	-12.7	14.1	5.4×10^{-5}	1.3×10^{10}
	L'→M	16.4	-10.5	5.9	7.2×10^{-5}	3.0×10^{9}
5a$_2$-H$_a^+$	**K→L'**	1.1	0.9	2.0	3.6×10^{-4}	1.7×10^{9}
	K→M	6.2	-4.1	2.1	5.6×10^{-5}	2.8×10^{8}
	L'→M	43.6	-21.1	22.6	7.4×10^{-5}	4.5×10^{10}
5a$_2$-H$_b^+$	**K→L'**	1.9	0.6	2.5	3.6×10^{-4}	2.6×10^{9}
	K→M	23.8	-11.5	12.2	5.5×10^{-5}	9.7×10^{9}
	L'→M	11.9	-7.0	4.9	7.3×10^{-5}	2.1×10^{9}
5a$_1$-H$_2^{2+}$	**K→L'**	29.4	-13.9	15.5	3.6×10^{-4}	1.0×10^{11}
	K→M	12.4	-4.0	8.3	1.4×10^{-4}	1.2×10^{10}
	L'→M	24.5	-9.3	15.2	2.1×10^{-4}	5.8×10^{10}
5a$_2$-H$_2^{2+}$	**K→L'**	1.5	0.7	2.2	3.6×10^{-4}	2.0×10^{9}
	K→M	9.2	-2.8	6.4	1.4×10^{-4}	6.9×10^{9}
	L'→M	8.0	-2.9	5.1	2.1×10^{-4}	6.7×10^{9}
5b$_1$	**K→M'**	12.1	-6.6	5.5	1.2×10^{-4}	4.3×10^{9}
	K→M'	5.4	-1.0	4.4	2.2×10^{-4}	4.9×10^{9}
	M'→L	17.7	-7.8	9.9	4.1×10^{-4}	4.7×10^{10}
5b$_2$	**K→M'**	14.4	-7.5	6.6	1.2×10^{-4}	6.1×10^{9}
	K→M'	38.1	-17.5	20.6	2.2×10^{-4}	1.1×10^{11}
	M'→L	7.2	-2.1	5.1	4.0×10^{-4}	1.2×10^{10}
5b$_1$-H$^+$	**K→L**	10.6	-5.9	4.7	1.2×10^{-4}	3.1×10^{9}
	K→M'	1.1	-1.8	-0.7	3.2×10^{-4}	2.1×10^{8}
	M'→L	10.8	-5.0	5.8	2.1×10^{-4}	8.1×10^{9}
5b$_2$-H$^+$	**K→L**	12.9	-7.0	5.9	1.2×10^{-4}	4.8×10^{9}
	K→M'	29.0	-13.8	15.1	3.2×10^{-4}	8.7×10^{10}
	M'→L	2.5	-0.2	2.3	2.0×10^{-4}	1.3×10^{9}

Table S10 Follow-up of Table S9

Molecule	D→A	V^{Coul}	V^{PCM}	V^{Tot}	J	$k^{th.}$
5c$_1$	**K→L'**	4.8	-3.4	1.4	3.6×10^{-4}	8.0×10^{8}
	K→M'	5.3	-1.1	4.2	2.2×10^{-4}	4.5×10^{9}
	L'→M'	80.3	-39.8	40.5	2.8×10^{-4}	5.5×10^{11}
5c$_2$	**K→L'**	0.2	-1.4	-1.2	3.6×10^{-4}	6.1×10^{8}
	K→M'	38.9	-18.0	20.9	2.2×10^{-4}	1.1×10^{11}
	L'→M'	44.7	-23.8	20.9	2.8×10^{-4}	1.5×10^{11}
5c$_3$	**K→L'**	27.1	-13.1	14.0	3.6×10^{-4}	8.4×10^{10}
	K→M'	40.1	-18.5	21.6	2.2×10^{-4}	1.2×10^{11}
	L'→M'	24.9	-17.5	7.4	2.8×10^{-4}	1.8×10^{10}
5c$_4$	**K→L'**	28.6	-13.8	14.8	3.6×10^{-4}	9.4×10^{10}
	K→M'	4.3	-0.7	3.6	2.1×10^{-4}	3.4×10^{9}
	L'→M'	31.6	-18.6	13.0	2.8×10^{-4}	5.6×10^{10}
5c$_1$**-H**$^+$	**K→L'**	0.8	0.9	1.7	3.6×10^{-4}	1.3×10^{9}
	K→M'	25.7	-9.7	16.0	3.2×10^{-4}	9.7×10^{10}
	L'→M'	29.4	-16.6	12.8	1.5×10^{-4}	2.9×10^{10}
5c$_2$**-H**$^+$	**K→L'**	1.0	-1.8	-0.8	3.6×10^{-4}	2.6×10^{8}
	K→M'	32.3	-15.2	17.1	3.2×10^{-4}	1.1×10^{11}
	L'→M'	20.2	-11.5	8.7	1.4×10^{-4}	1.2×10^{10}
5c$_3$**-H**$^+$	**K→L'**	6.0	-3.7	2.3	3.6×10^{-4}	2.3×10^{9}
	K→M'	36.0	-17.0	19.1	3.2×10^{-4}	1.4×10^{11}
	L'→M'	1.0	-5.6	-4.6	1.4×10^{-4}	3.6×10^{9}
5c$_4$**-H**$^+$	**K→L'**	5.7	-3.8	1.9	3.6×10^{-4}	1.5×10^{9}
	K→M'	22.1	-8.3	13.8	3.2×10^{-4}	7.2×10^{10}
	L'→M'	66.7	-35.7	35.7	1.5×10^{-4}	2.3×10^{11}

S12 Choice of designed compounds with a link at β position

In this Section, we discuss the choice adopted for designing new compounds with BODIPYs at β position. In Figures S15, S16 and S17, we report the transition energies and NTO orbitals for the first three excited-states of : (i) compound **4**, in which the BODIPY units are linked to the triethynylbenzene through *meso* phenyls); (ii) compound **4-β**, in which the BODIPY fragments are directly attached to the triethynylbenzene core and (iii) molecule **7**, in which the ethynyl groups of **4-β** have been replaced with phenyl rings. In this latter case, the phenyl rings are added in the definition of the fragments, that therefore present different labels than in **4** and **4-β**. As already shown for the reference molecule **1a**, the excited-states of **4** are purely localized on the BODIPY fragments. In contrast, when directly attaching the BODIPY moieties to the triethynyl core (**4-β**), the excited-states are found to be partially delocalized over the ethynyl bridge indicating that our model will become less suited for **4-β** than for other molecules. One can modify the BODIPY units inserting a phenyl at β position in order to decouple the fragments from the core. We have therefore chosen this approach in the last design part.

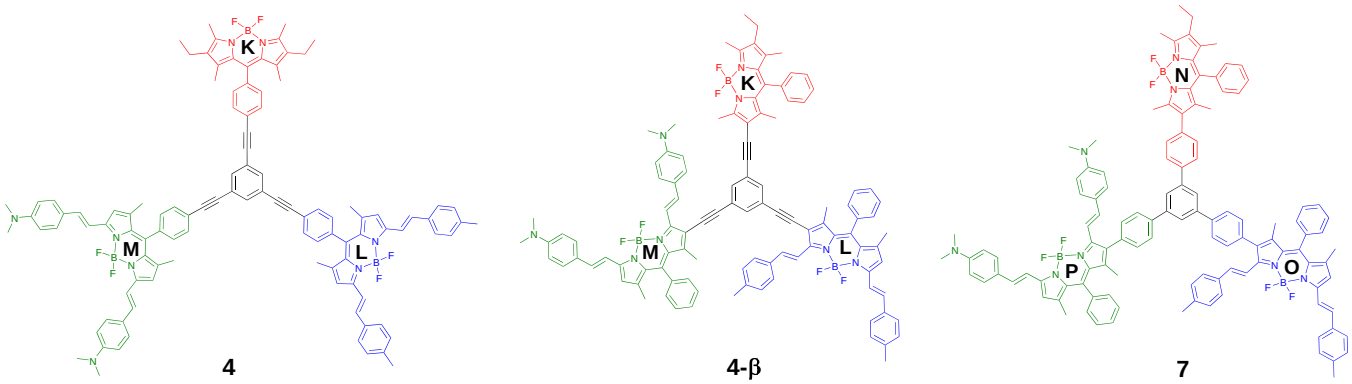

Fig. S14 Representation of the structures investigated in this Section.

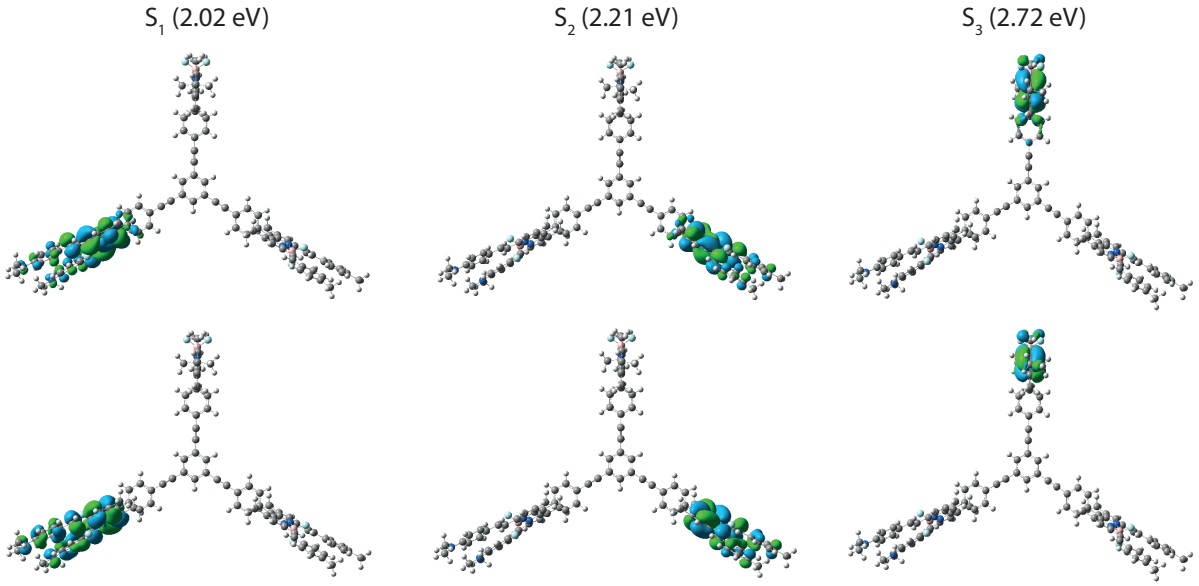

Fig. S15 The dominant natural transition orbital pairs (isovalue=0.02 a.u.) for the first three singlet excited-states of **4**. In parenthesis, we report the corresponding transition energies. For each state, the "hole" is at the top, the "particle" at the bottom. The associated eigenvalues are 0.970, 0.980, 0.996 for S_1, S_2 and S_3, respectively.

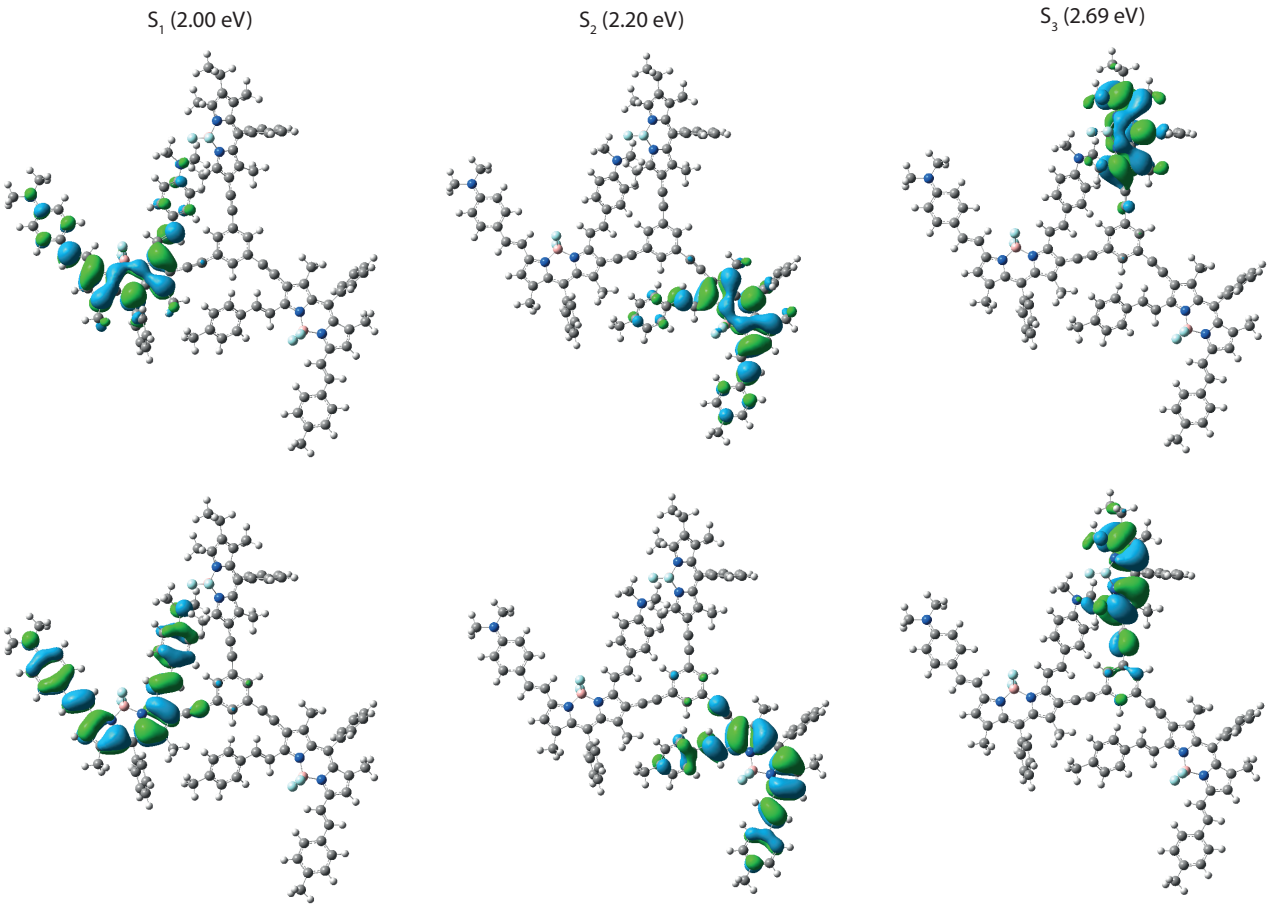

Fig. S16 The dominant natural transition orbital pairs (isovalue=0.02 a.u.) for the first three singlet excited-states of **4-β**. For each state, the "hole" is at the top, the "particle" at the bottom. The associated eigenvalues are 0.951, 0.960, 0.981 for S_1, S_2 and S_3, respectively.

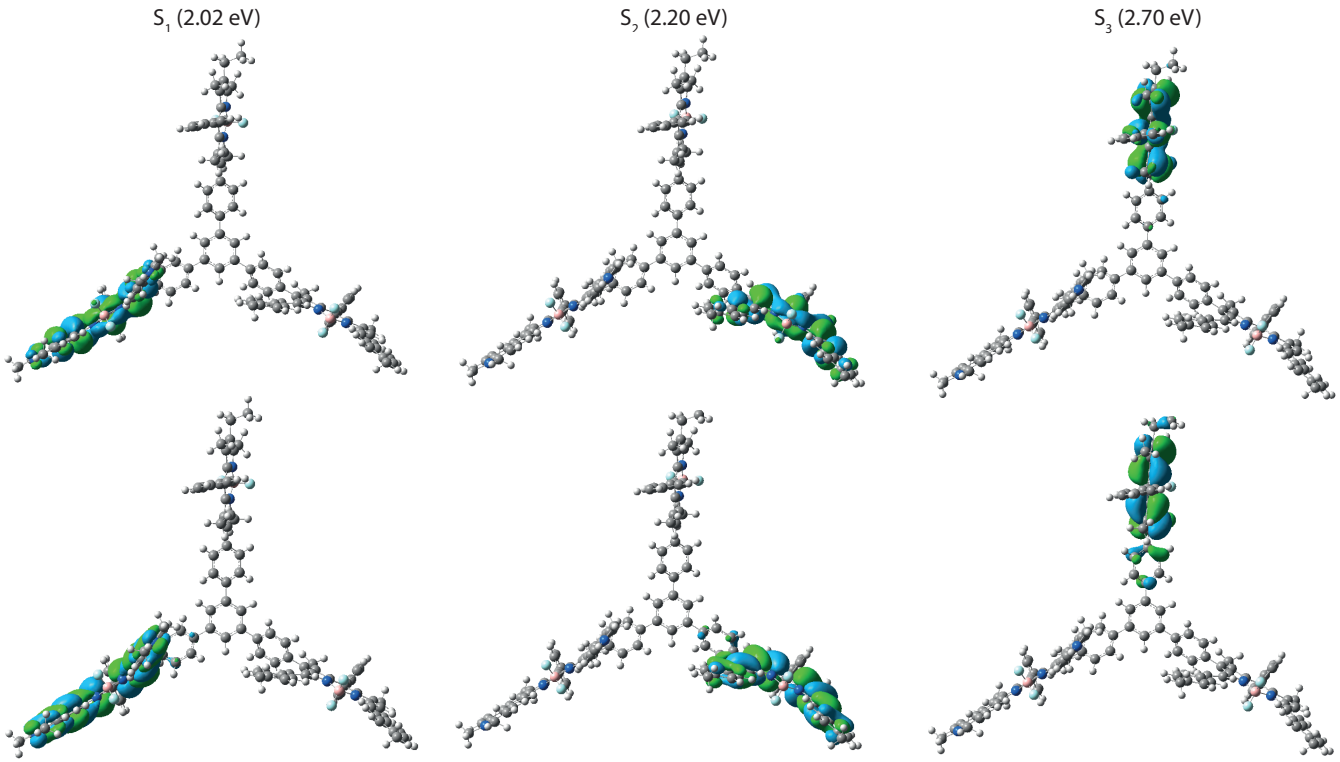

Fig. S17 The dominant natural transition orbital pairs (isovalue=0.02 a.u.) for the first three singlet excited-states of **7**. In parenthesis, we report the corresponding transition energies. For each state, the "hole" is at the top, the "particle" at the bottom. The associated eigenvalues are 0.964, 0.973, 0.989 for S_1, S_2 and S_3, respectively.

S13 Additional data for structures 6 and 7

In Table S10, we report the transition energies of each fragment in the designed triads derived from **6** and **7**. See Figures S18 and S19 for representation.

Table S11 Comparison between the electronic transition energy ($E^{X}_{S_1}$ in eV) of each fragment in triad **6** and **7**

Molecule	$E_{rel.}$	$E^{K}_{S_1}$	$E^{L}_{S_1}$	$E^{M}_{S_1}$
6d	0.01	2.71	2.21	2.02
6e	0.05	2.71	2.21	2.02
6f	0.00	2.71	2.21	2.02
6g	0.03	2.71	2.21	2.02
7d	0.02	2.71	2.21	2.02
7e	0.01	2.71	2.21	2.02
7f	0.02	2.71	2.20	2.02
7g	0.00	2.71	2.21	2.02

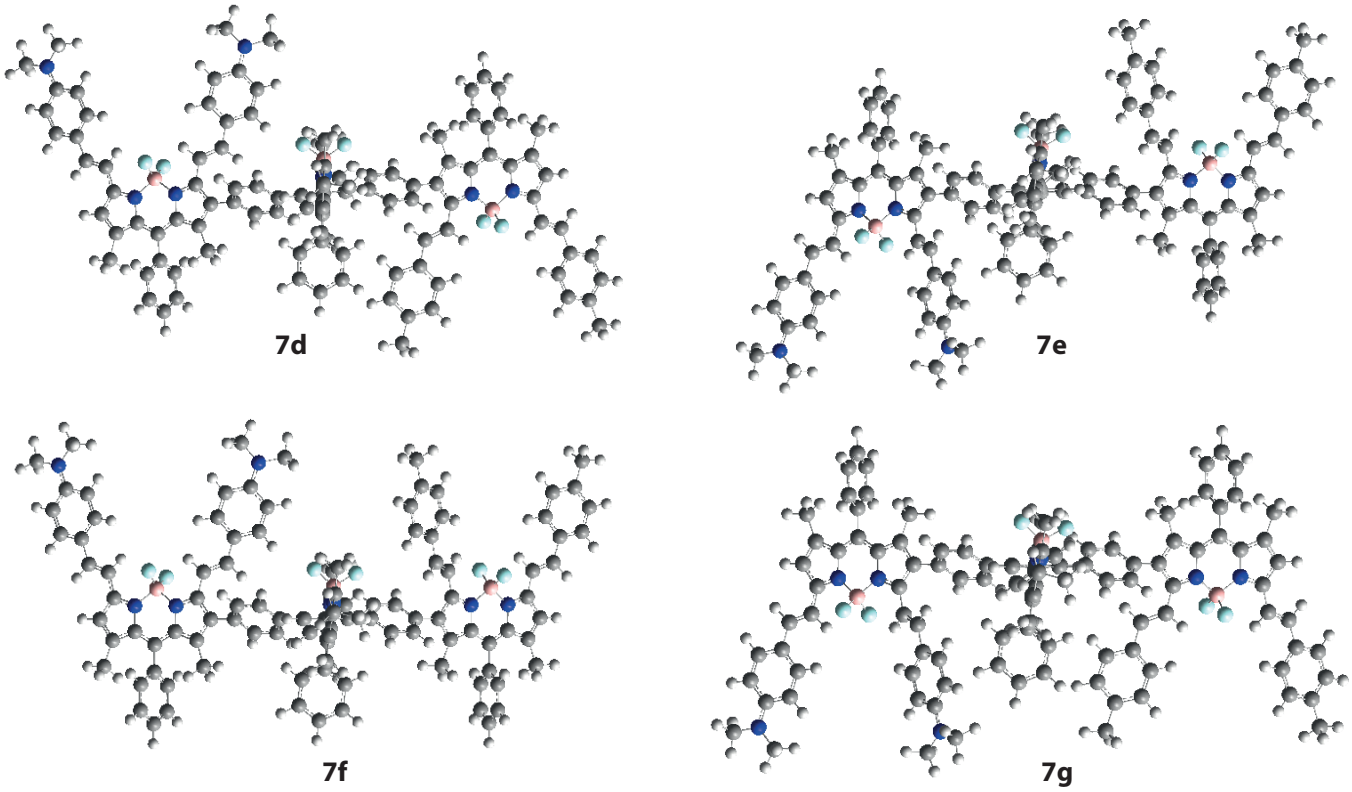

Fig. S18 Representation of the optimized conformers of molecule **6**.

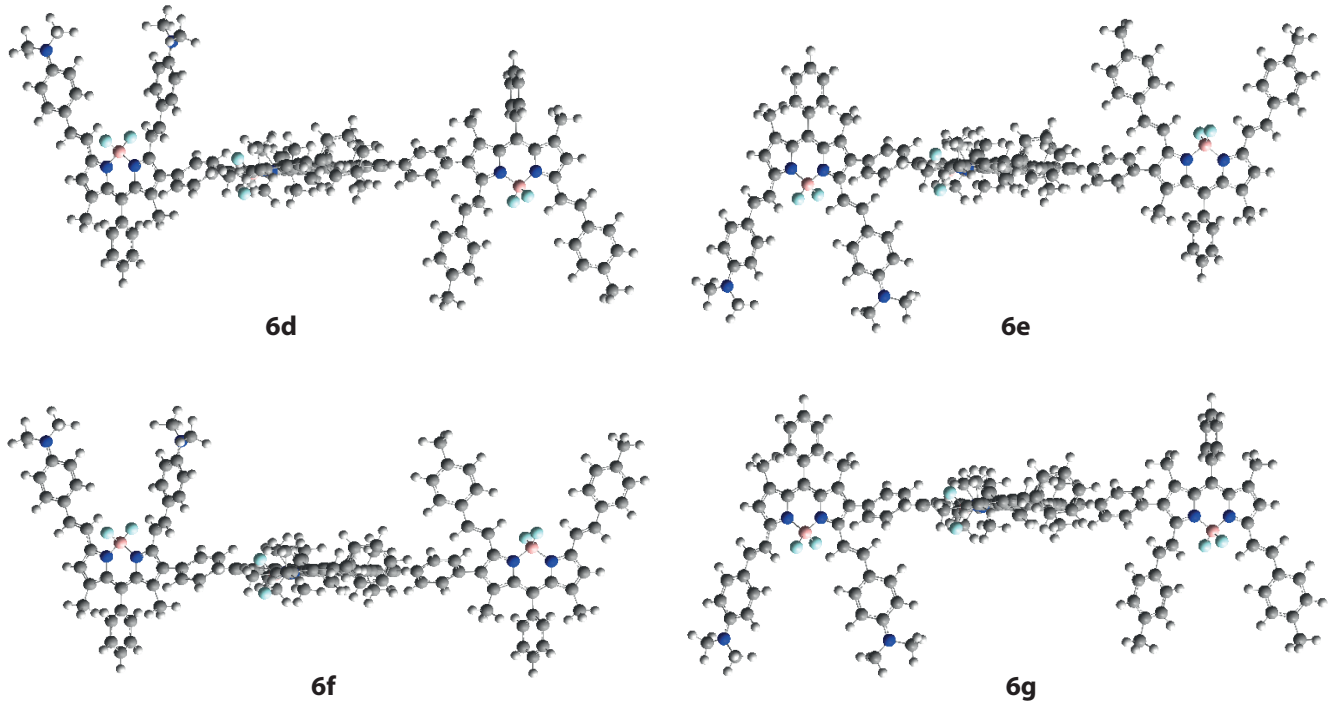

Fig. S19 Representation of the optimized conformers of molecule **7**.

Table S12 Theoretical couplings (V in cm^{-1}), spectral overlap (J in cm) and EET rate constants ($k^{th.}$ in s^{-1}) in **6** and **7** (see Figure 7 in the body of the text). The directionality of the energy transfer from the donor part (D) to the acceptor part (A), denoted D→A, is reported according to the computed transition energies (see Table S11). The rotational conformers of **6** and **7** are displayed in Figures S18 and S19, respectively

Molecule	D→A	V^{Coul}	V^{PCM}	V^{Tot}	J	$k^{th.}$
6d	**N→O**	58.3	-31.3	27.0	1.3×10^{-4}	1.1×10^{11}
	N→P	59.5	-31.8	27.7	3.7×10^{-5}	3.4×10^{10}
	O→P	60.3	-33.2	27.1	2.7×10^{-4}	2.3×10^{11}
6e	**N→O**	53.5	-29.3	24.3	1.3×10^{-4}	8.9×10^{10}
	N→P	56.9	-30.8	26.1	3.7×10^{-5}	3.0×10^{10}
	O→P	67.0	-36.0	31.0	2.7×10^{-4}	3.0×10^{11}
6f	**N→O**	53.1	-29.1	24.0	1.3×10^{-4}	8.9×10^{10}
	N→P	59.5	-31.7	27.8	3.8×10^{-5}	3.4×10^{10}
	O→P	69.6	-37.3	32.2	2.6×10^{-4}	3.3×10^{11}
6g	**N→O**	58.1	-31.1	27.0	1.3×10^{-4}	1.1×10^{11}
	N→P	57.3	-31.0	26.4	3.8×10^{-5}	3.1×10^{10}
	O→P	74.9	-39.9	35.0	2.7×10^{-4}	3.9×10^{11}
7d	**N→O**	151.7	-75.6	76.0	1.3×10^{-4}	8.7×10^{11}
	N→P	149.4	-74.1	75.2	3.7×10^{-5}	2.5×10^{11}
	O→P	163.6	-81.1	82.4	2.7×10^{-4}	2.1×10^{12}
7e	**N→O**	166.0	-81.9	84.0	1.3×10^{-4}	1.1×10^{12}
	N→P	157.1	-77.1	80.0	3.7×10^{-5}	2.8×10^{11}
	O→P	147.4	-74.6	72.8	2.7×10^{-4}	1.7×10^{12}
7f	**N→O**	165.1	-81.3	83.8	1.3×10^{-4}	1.0×10^{12}
	N→P	149.1	-74.2	74.9	3.7×10^{-5}	2.4×10^{11}
	O→P	195.6	-97.3	98.3	2.7×10^{-4}	3.1×10^{12}
7g	**N→O**	151.8	-76.5	75.3	1.3×10^{-4}	8.5×10^{11}
	N→P	158.2	-78.5	79.7	3.7×10^{-5}	2.8×10^{11}
	O→P	192.3	-96.2	96.1	2.7×10^{-4}	2.9×10^{12}